# Simultaneous achievement of energy-efficient operation and high thermal stability of magnetic devices by enhancement of Dzyaloshinskii-Moriya interaction and magnetic anisotropy energy

Yong-Keun Park,[1,2,*,†] Minhwan Kim,[1,2,*] Joo-Sung Kim,[2,†] Yune-Seok Nam,[2,†] Ji-Sung Yu,[2] Jung-Hyun Park,[2] Jaesung Yoon,[2] Duck-Ho Kim,[1] Sug-Bong Choe,[2,‡] and Byoung-Chul Min[1,§]

[1]*Center for Spintronics, Korea Institute of Science and Technology, Seoul 02792, Republic of Korea*

[2]*Department of Physics and Institute of Applied Physics, Seoul National University, Seoul 08826, Republic of Korea*

(Received 29 March 2022; accepted 20 March 2024; published 16 April 2024)

Energy-efficient operation and stable data retention are the key features of magnetic information devices. Simultaneous achievement of writing-energy reduction and data-stability enhancement has yet faced a dilemma, since both are subjected to the same governing mechanism of magnetization switching, and thus, it is not easy to reduce writing energy while keeping high thermal stability. Here, we propose a solution that bypasses the dilemma by introducing chiral spin alignment in magnetic structures, which assists the current-induced switching at pattern edges, with the energy barrier enhancement. Experiments on asymmetric Pt/Co/Cu/Pt films reveals that both the Dzyaloshinskii-Moriya interaction (DMI) and perpendicular magnetic anisotropy (PMA) are increased by inserting an ultrathin Cu layer. A large PMA enhances the thermal stability, whereas a large DMI reduces the switching current density by tilting the angle of chiral spin alignment at pattern edges. The present observation shows that an effective DMI engineering provides energy-efficient and highly stable magnetic structures suitable for spintronic applications.

DOI: 10.1103/PhysRevMaterials.8.044405

## I. INTRODUCTION

Current-induced magnetization dynamics with spin-transfer torque (STT) or spin-orbit torque (SOT) enables us to realize magnetic devices based on the electrical control of magnetization states [1–5]. The STT- or SOT-driven magnetization switching provides building blocks of emerging magnetic memory, logic, and many other types of information devices.

The most important challenges of these magnetic devices are to achieve sufficiently high thermal stability, and simultaneously low switching current density. The high thermal stability is required to avoid unwanted switching by thermal fluctuation. The thermal stability factor $\Delta$ ($= K_U V/k_B T$) should be larger than about 40 to secure the data retention over 10 years [6], where $K_U$ is the uniaxial magnetic anisotropy, $V$ is the volume of a storage magnet, $k_B$ is the Boltzmann constant, and $T$ is the temperature. In order to decrease $V$ for high density storage devices, $K_U$ has to be enhanced accordingly to sustain the proper magnitude of $\Delta$ to resist the thermal fluctuation energy $k_B T$. On the other hand, a large $K_U$ inevitably increases the switching current density through the enhancement of energy barrier height between magnetic states. Therefore, it is difficult to achieve both the thermal stability and switching efficiency simultaneously.

Recent studies have revealed that the Dzyaloshinskii-Moriya interaction (DMI) can play a key role in magnetization switching via domain nucleation [7–9]. These results suggest that the DMI engineering of magnetic materials possibly provides an opportunity to control the switching current irrespective of the thermal stability [8,10]. Since the magnetization switching assisted by the DMI appears to be initiated at pattern edges [7,8], the precise structure engineering as well as detailed study of the current-induced switching at pattern edges are required.

To clearly demonstrate the relation between the switching current density and the DMI strength, it is required to control the DMI strength over a wide range. For this purpose, we designed a series of layer stacks of Pt/Co/Cu/Pt, where an ultrathin Cu layer is inserted to symmetric Pt/Co/Pt. The Cu insertion layer was selected because an ultrathin Cu insertion layer on top of Co does not decrease the perpendicular magnetic anisotropy (PMA), and it maintains strong PMA even with thin Co layers [11,12]. Since the DMI strength strongly depends on the interface and layer thickness [7,13,14], a drastic change of DMI is expected with the insertion of Cu layers. To avoid the current shunt to the insertion layer, we limited the thickness of the Cu insertion layers less than or equal to 0.4 nm. Then, by measuring the energy barrier and switching current density in addition to the strengths of PMA and DMI of the series of films, we demonstrated that it is possible to simultaneously achieve both thermal-stability enhancement and switching-current reduction.

## II. SAMPLE PREPARATION AND MAGNETIC CHARACTERIZATION

The layer stack of the samples consists of 5-nm Ta/8-nm Pt/0.3-nm Co/$t_{Cu}$ Cu/1.5-nm Pt with different Cu layer thicknesses ($t_{Cu}$ = 0, 0.1, 0.2, 0.3, and 0.4 nm). All samples were

*These authors contributed equally to this work.
†Present address: Samsung Electronics Co., Ltd.
‡sugbong@snu.ac.kr
§min@kist.re.kr

 

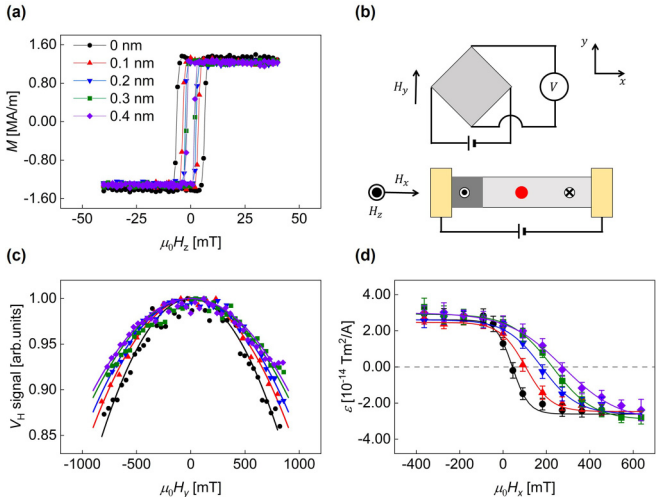


FIG. 1. (a) The easy-axis hysteresis loop measured by vibrating sample magnetometer. (b) The schematics for measuring the magnetic anisotropy field $\mu_0 H_K$ (upper part) and SOT efficiency $\varepsilon$ (bottom part), respectively. In the bottom part, the red dot denotes the laser spot for the MOKE signal and the yellow squares indicate the electrodes for current injection. (c) The normalized anomalous Hall effect signal $V_H$ with respect to $\mu_0 H_y$. The symbols are measured data and solid lines are fitting lines. (d) Plots of $\varepsilon$ with respect to $\mu_0 H_x$. The vertical error bars are the standard deviation of several repeated measurements. The grey horizontal line indicates $\varepsilon = 0$. The curved solid lines guide the eyes. All black, red, blue, dark green, and violet symbols and lines correspond to the samples with Cu 0, 0.1, 0.2, 0.3, and 0.4 nm, respectively.

deposited by dc-magnetron sputtering on Si wafers with a 100-nm-thick $SiO_2$ layer. The lowermost Ta is employed as a seed layer. To measure the strengths of the SOT and DMI, 20-μm-wide and 350-μm-long microwires were patterned by photolithography and ion-milling processes. To inject electric current into the microwires, 5-nm Ta/90-nm Au electrodes were deposited and patterned by lift-off process.

The magnetic properties of the films were then characterized by vibrating sample magnetometer. Figure 1(a) shows the easy-axis hysteresis loops of the magnetization $M$ with respect to out-of-plane magnetic field $\mu_0 H_z$, confirming that the saturation magnetization $M_S$ remains almost unchanged with varying the Cu thickness from 0 to 0.4 nm.

The magnetic anisotropy field $\mu_0 H_K$ of the films were investigated by the anomalous Hall effect (AHE) measurements. Schematic illustration of the experiment is shown in the upper part of Fig. 1(b). Figure 1(c) plots the AHE signal $V_H$ with respect to in-plane magnetic field $\mu_0 H_y$, which is transverse to the current direction, under a fixed $\mu_0 H_z$ bias. Here, $V_H$ is proportional to the out-of-plane component $m_z$ of the magnetization, i.e., $V_H \propto m_z (= \cos\theta)$ with the polar angle $\theta$ from the out-of-plane axis. When both $\mu_0 H_y$ and $\mu_0 H_z$ are applied to the film, the magnetization angle $\theta$ is determined as $\cos\theta \cong 1 - [\mu_0 H_y/2(\mu_0 H_K + \mu_0 H_z)]^2$, where $\mu_0 H_K$ is the magnetic anisotropy field, based on the Stoner-Wohlfarth theory within lowest order Taylor expansion [15–17]. Then, by fitting the experimental data to the equation, $\mu_0 H_K$ can be estimated. A rapid decrease of $V_H$ with increasing $\mu_0 H_y$ indicates a smaller $\mu_0 H_K$. The films with a thicker $t_{Cu}$ show a larger $\mu_0 H_K$ and thus a larger effective magnetic-anisotropy-energy density $K_U^{eff}$ $(= \mu_0 M_S H_K/2)$.

The DMI-induced effective magnetic field $\mu_0 H_{DMI}$ was also quantified by the measurement of the SOT efficiency $\varepsilon$ with respect to $\mu_0 H_x$. The domain was initially nucleated at a nucleation pad and we swept the perpendicular $\mu_0 H_z$ under the application of a fixed current bias. When the domain wall (DW) reached the position of the laser spot for the detection of the magneto-optical Kerr effect (MOKE) signal [see schematic illustration shown in the bottom part of Fig. 1(b)], one can observe a sign inversion in the MOKE signal (see the red spot) indicating the depinning field $\mu_0 H_{dep}$. By measuring $\mu_0 H_{dep}$ with respect to various current density $J$, $\varepsilon$ was measured [18,19]. The measured $\varepsilon$ with respect to $\mu_0 H_x$ is shown in Fig. 1(d). According to Ref. [19], the strength of $\mu_0 H_{DMI}$ can be obtained from the intercept to the $x$ axis (i.e., $\varepsilon = 0$); the magnitude of the SOT efficiency $\varepsilon_0$ can be determined from the saturation value of $\varepsilon$. The detailed measurement method and the analysis are provided in Note 1 of the Supplemental Material [20]. As $t_{Cu}$ increases from 0 to 0.4 nm, $\mu_0 H_{DMI}$ increases significantly from zero to finite magnitudes, whereas $\varepsilon_0$ remains almost constant with variation of 7.4%. Table I summarizes all the measured values of $M_S$, $\mu_0 H_K$, $K_U^{eff}$, $\mu_0 H_{DMI}$, and $\varepsilon_0$.

## III. RESULTS AND DISCUSSION

### A. Field-induced magnetization switching

The thermal stability of the films depends on the magnitude of switching energy barrier, which can be directly measured by field-induced magnetization switching. For this measurement, a circular dot structure of Co/Cu/Pt (6 μm in diameter) was patterned on the center of a Hall cross bar of Ta/Pt (10 μm in width) as depicted by Fig. 2(a). Then, the perpendicular magnetization $m_z$ of the circular dot was observed by monitoring the AHE signal $V_H$ $(\propto m_z)$. The current density $J$ for the AHE measurement was kept as low as possible to avoid unwanted effects from the SOT-induced effective magnetic field, which is estimated to be negligibly small (less than 0.03 mT) with the used current density $(J \leqslant 1.1\times10^9\ \mathrm{A/m^2})$.

The magnetization switching probability $P$ is then measured with respect to time $t$ under various strength of $\mu_0 H_z$. Figures 2(b)–2(f) show the plots of $P$ with respect to $t$ for the films with different $t_{Cu}$ as denoted in each panel. For each fixed $\mu_0 H_z$, it is clear from the plots that $P$ follows an exponential decay with

$$P = 1 - \exp(-t/\tau), \tag{1}$$

where the half-decay time $\tau$ is known to follow the Arrhenius law as given by

$$\tau = \tau_0 \exp(E_B/k_B T). \tag{2}$$

Here, $\tau_0$ is the characteristic time (or inverse of attempt frequency) [21,22] and $E_B$ is the energy barrier for magnetization switching. Therefore, the measurement of switching probability as a function of time allows us to estimate $\tau$ and $E_B$. For a quantitative comparison, $\ln\tau$ is plotted with respect to $(1/\mu_0 H_z - 1/\mu_0 H_0)$ for the series of film [Fig. 2(g)]. It is clear from the plot that $\tau$ increases as $t_{Cu}$ increases. These

TABLE I. Magnetic properties of the 5-nm Ta/8-nm Pt/0.3-nm Co/$t_{Cu}$ Cu/1.5-nm Pt samples with different Cu layer thicknesses ($t_{Cu}$).

| $t_{Cu}$ (nm) | $M_S$ (MA/m) | $\mu_0 H_K$ (T) | $K_U^{eff}$ ($10^6$ J/m$^3$) | $\mu_0 H_{DMI}$ (mT) | $\varepsilon_0$ ($10^{-14}$ Tm$^2$/A) |
|---|---|---|---|---|---|
| 0 | $1.33 \pm 0.03$ | $1.49 \pm 0.02$ | $0.99 \pm 0.04$ | $-28.55 \pm 6.87$ | $2.61 \pm 0.13$ |
| 0.1 | $1.32 \pm 0.02$ | $1.69 \pm 0.02$ | $1.12 \pm 0.03$ | $-93.58 \pm 13.35$ | $2.47 \pm 0.14$ |
| 0.2 | $1.30 \pm 0.03$ | $1.81 \pm 0.01$ | $1.18 \pm 0.03$ | $-149.00 \pm 13.88$ | $2.61 \pm 0.21$ |
| 0.3 | $1.32 \pm 0.02$ | $1.91 \pm 0.02$ | $1.26 \pm 0.03$ | $-228.85 \pm 9.70$ | $2.93 \pm 0.21$ |
| 0.4 | $1.31 \pm 0.03$ | $2.01 \pm 0.02$ | $1.32 \pm 0.04$ | $-234.47 \pm 16.04$ | $2.99 \pm 0.27$ |

observations therefore reveal that $E_B$ is enhanced with the Cu layer insertion.

The $E_B$ strongly depends on the specific switching mechanisms. For the case that the magnetization switching is governed by "coherent magnetization rotation," the $E_B$ is directly proportional to $K_U^{eff}$ [6]. Thus, a larger energy barrier and consequently larger thermal stability are expected for the films with a larger $K_U^{eff}$. On the other hand, for the case that the magnetization switching is governed by "domain nucleation," the $E_B$ is associated with the DW energy density $\sigma_{DW}$; the $E_B$ of the domain nucleation is proportional to $\sigma_{DW}^2$ [9,21,23].

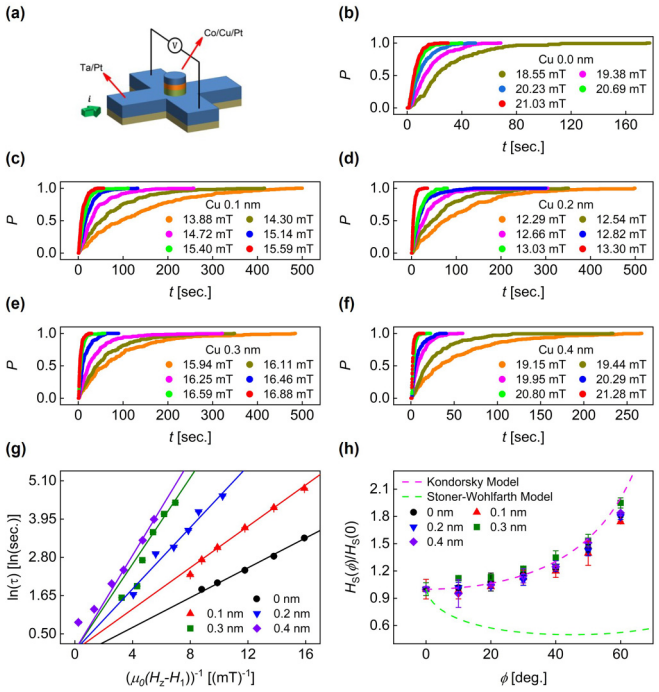


FIG. 2. (a) Schematic illustration of sample structure. A 6-μm-diameter Co/Cu/Pt circular dot is patterned on a 10-μm-width Ta/Pt cross Hall bar. (b)–(f) The switching probability $P$ with respect to field induction time $t$ for several different constant external fields $\mu_0 H_z$ as denoted inside each panel. The Cu thickness is also denoted in each panel. (g) The plot of $\ln(\tau)$ with respect to the $(1/\mu_0 H_z - 1/\mu_0 H_0)$. The symbols are measured data and solid lines are linear fitting lines. (h) The relative switching field with respect to the angle of applied external field. The magenta dashed line is the estimated trend from the Kondorsky model, and the green dashed line is from the Stoner-Wohlfarth model. In (g) and (h), all black, blue, red, dark green, and violet symbols and lines correspond to the samples with Cu 0, 0.1, 0.2, 0.3, and 0.4 nm, respectively.

According to Ref. [24], $\sigma_{DW}$ is given as $\sigma_{DW} = 4\sqrt{A_{ex} K_U^{eff}} - \pi \lambda \mu_0 H_{DMI} M_S$ for the Néel-type DWs, where $A_{ex}$ is the exchange stiffness and $\lambda$ $(= \sqrt{A_{ex}/K_U^{eff}})$ is the DW width [4]. The $E_B$ of the domain nucleation has nontrivial dependence on $K_U^{eff}$ with an additional term of $\mu_0 H_{DMI}$. The validation of the analysis is affirmed by the presence of Néel-type DWs in all film series, as substantiated in Note 2 of the Supplemental Material [20]. Consequently, in order to understand the origin of the $E_B$ enhancement, detailed switching mechanisms are to be examined.

To explore the most dominant switching mechanism in our series of films, the switching magnetic field $\mu_0 H_S$ was measured with respect to the angle $\phi$ of the external magnetic field, where $\phi$ is the angle from the $z$ axis on the $zy$ plane. In general, two models are employed to comprehend magnetization switching: the Stoner-Wohlfarth model and the Kondorsky model [15,25]. The Stoner-Wohlfarth model, employed for coherent magnetization rotation, describes a scenario where initially parallel magnetizations, pointing in opposite directions, abruptly switch directions. The switching field adheres to the relation $\mu_0 H_S(\phi)/\mu_0 H_S(0) = (1 - t^2 + t^4)^{1/2}/(1 + t^2)$, where $t = \tan^{1/3}\phi$ [15]. Conversely, the Kondorsky model elucidates magnetization reversal through the expansion of the domain with an initial state of pinned DW. The switching field follows the relation $\mu_0 H_S(\phi)/\mu_0 H_S(0) = 1/\cos\phi$ [25]. The measured data shown in Fig. 2(h) are compared with the theoretical predictions by the Stoner-Wohlfarth model (green dashed line) and the Kondorsky model (magenta dashed line). The comparison with theoretical models manifests that the magnetization switching occurs by the domain nucleation for all the series of films.

It is worthwhile to note that the linear dependence of $\ln\tau$ with respect to $(\mu_0 H_z)^{-1}$ in Fig. 2(g) also indicates the domain-nucleation-dominant switching mechanism. The magnetic droplet model describes the magnetization reversal process via the nucleation of circular domain, followed by the propagation of DWs [9,21,23]. According to the magnetic droplet model of the domain nucleation at edges, $E_B$ follows the relation

$$E_B = \Lambda\left(\frac{1}{\mu_0 H_z} - \frac{1}{\mu_0 H_0}\right) \quad \text{with } \Lambda = \frac{\pi \sigma_{DW}^2 t_{Co}}{4 M_S}, \qquad (3)$$

where $t_{Co}$ is the Co layer thickness and $\mu_0 H_0$ is the maximum coercive field ($\cong \mu_0 H_K$) as proposed in Ref. [23]. Using Eq. (2), the linear relation between $\ln\tau$ and

TABLE II. Estimated Λ of a circular dot structure of Co/Cu/Pt obtained with two different measurement methods.

| $t_{Cu}$ (nm) | Λ ($10^{-21}$ JT) (switching probability measurement) | Λ ($10^{-21}$ JT) (coercivity measurement) |
|---|---|---|
| 0 | $0.95 \pm 0.0002$ | $1.02 \pm 0.16$ |
| 0.1 | $1.27 \pm 0.0003$ | $1.15 \pm 0.35$ |
| 0.2 | $1.88 \pm 0.0004$ | $1.54 \pm 0.29$ |
| 0.3 | $2.65 \pm 0.0005$ | $2.48 \pm 0.99$ |
| 0.4 | $2.91 \pm 0.0024$ | $2.62 \pm 0.92$ |

$(1/\mu_0 H_z - 1/\mu_0 H_0)$ in Fig. 2(e) is well described by

$$\ln \tau = \frac{\Lambda}{k_B T}\left(\frac{1}{\mu_0 H_z} - \frac{1}{\mu_0 H_0}\right) + C, \tag{4}$$

with a constant $C$ $(= \ln \tau_0)$. From the best linear fit to Eq. (4), the magnitudes of Λ were estimated and then listed in Table II. To validate Λ, an independent measurement of Λ can be conducted using the coercivity measurement presented in Table II. This approach demonstrates a consistent agreement between the two independent measurements, with detailed information provided in Note 3 of the Supplemental Material [20].

### B. Current-induced DW motion

Next the switching current dependence on the DMI was characterized by observing the current-induced DW motion of a circular dot structure of Co/Cu/Pt [Fig. 2(a)]. In this experiment, we have measured the threshold current density $J_S$ by monitoring the magnetization switching while sweeping $J$ under a fixed $\mu_0 H_z$ bias. The switching loops with various $\mu_0 H_z$ bias of $t_{Cu} = 0.2$ nm are shown in Fig. 3(a). Figure 3(b) plots $J_S$ with respect to several different $\mu_0 H_z$ bias for the series of films (please note that the abscissa is scaled by $\mu_0 H_z/\mu_0 H_C$ to compensate for the $\mu_0 H_C$ variation among the films). The injected current to the Hall-bar geometry generates SOT equivalent to an effective magnetic field $\mu_0 H_z^{SOT}$ $(\propto J)$, and thus the magnetization switching occurs when the total magnetic field $(= \mu_0 H_z + \mu_0 H_z^{SOT})$ overcomes the $\mu_0 H_C$. Therefore, it is natural to expect that $J_S$ decreases as $\mu_0 H_z$ increases, as observed in Fig. 3(b). A salient feature of this experiment is that the $J_S$ with samples with a Cu insertion layer is significantly smaller than that without a Cu insertion layer.

The reduction of $J_S$ by inserting a Cu layer could be associated with a couple of possible origins. To check whether such $J_S$ reduction is related to $E_B$ variation with the Cu insertion layer, $E_B$ is plotted with respect to $\mu_0 H_z/\mu_0 H_C$ [Fig. 3(c)], where the magnitudes of $E_B$ at $T = 295$ K were determined by Eq. (3). The $E_B$ decreases more or less linearly with increasing $\mu_0 H_z$ [Fig. 3(c)], which is not the case for $J_S$ [Fig. 3(b)]. Moreover, the $E_B$ with samples with a Cu layer is much larger than the $E_B$ without a Cu insertion layer; the $E_B$ enhancement by the Cu insertion is exactly opposite to what we have observed with $J_S$ reduction. This result rules out a possibility that the $J_S$ reduction is attributed to the $E_B$ variation.

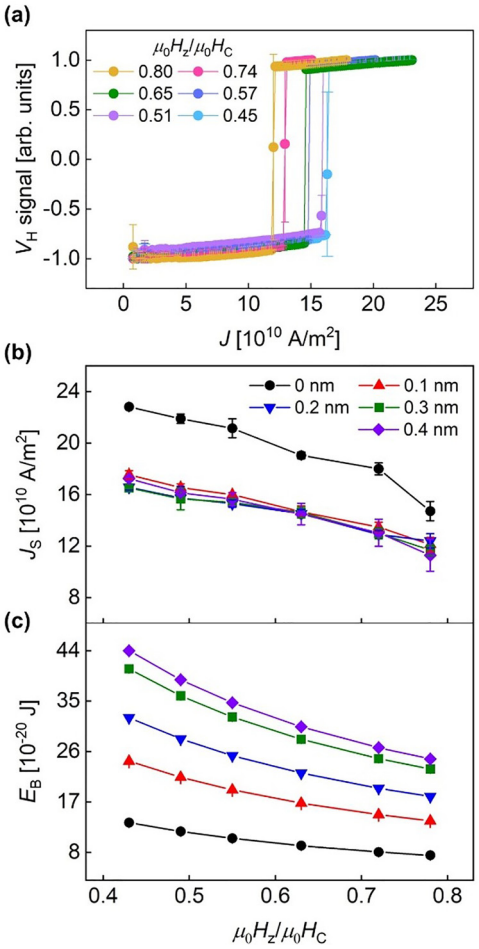


FIG. 3. (a) Current-induced magnetization switching loops with $H_z$ bias of $t_{Cu} = 0.2$ nm, measured by anomalous Hall voltage. As the larger $H_z$ was applied, $J_S$ decreased. Plot of (b) $J_S$ and (c) $E_B$ with respect to $H_z/H_C$ for different $t_{Cu}$ as denoted in each panel. In (b), the vertical error bars are the standard deviation of several repeated measurements. In (c), the vertical error bars are the error of the Λ determination from the measurement of $\tau$.

The effect of DMI could be a possible reason for the $J_S$ reduction. In the SOT theory [18], the strength of $\mu_0 H_z^{SOT}$ in a perpendicular magnet is proportional to the $x$ component of magnetization $m_x$. In materials with a large DMI, the DMI gives rise to chiral spin alignment which is maximized at the pattern edges due to the absence of neighboring spins at the boundaries. The magnetization switching is initiated by domain nucleation at the pattern edges [7–9,26]. To ensure the initial domain nucleation at the pattern edge, the MOKE image was taken at the 44-μm-dot of $t_{Cu} = 0.2$ nm. As a current pulse of $J = 1.06 \times 10^{11}$ A/m$^2$ with width of 30 ms was injected to the dot, the domain was nucleated at the left edge of the dot [Fig. 4(a)]. The detailed description of the domain nucleation at the edge with various current and domain polarities is provided in Fig. S4 in Note 4 of the Supplemental Material [20]. The largest $m_x$ and consequent largest $\mu_0 H_z^{SOT}$ [7–9] appear at the pattern edges, and the magnitude of $m_x$ is proportional to $\mu_0 H_{DMI}/\mu_0 H_K$ [9]. The larger the $m_x$, the smaller the $J_S$. Figure 4(b) shows $J_S$ with

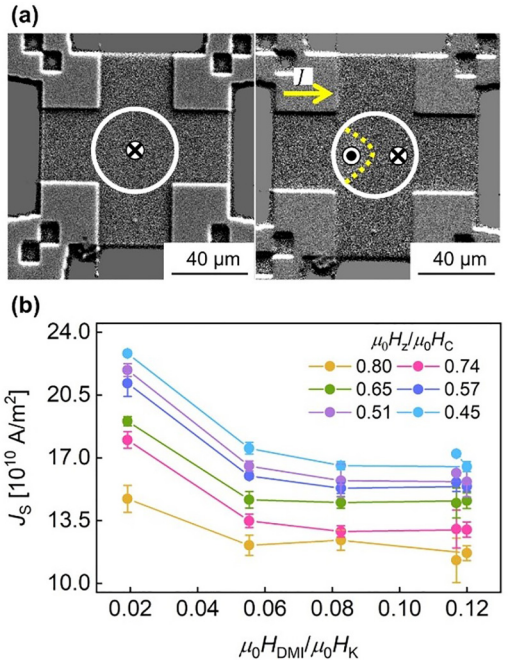


FIG. 4. (a) The MOKE images about the domain nucleation procedure at the edge. The image was taken at the 44-μm dot of $t_{Cu} = 0.2$ nm. The dot was initially saturated to the down domain (left part) and the up domain was nucleated by SOT due to chiral spin alignment at the edge (right part). The current pulse of amplitude $J = 1.06\times10^{11}$ A/m$^2$ with width of 30 ms was injected. The bright (dark) state corresponds to the up (down) domain. (b) Plot of $J_S$ with respect to $\mu_0H_{DMI}/\mu_0H_K$ with several different $\mu_0H_z/\mu_0H_C$ as denoted in the panel. The samples ranging from the smallest $\mu_0H_{DMI}/\mu_0H_K$ to the largest $\mu_0H_{DMI}/\mu_0H_K$ indicate that with Cu 0, 0.1, 0.2, 0.3, and 0.4 nm, in ascending order. The vertical error bars are the standard deviation of several repeated measurements and the horizontal error bars are estimated from the chi fitting errors of $\mu_0H_{DMI}$ and $\mu_0H_K$. In (b), the vertical error bars are the error of the $\Lambda$ determination from the measurement of $\tau$.

respect to $\mu_0H_{DMI}/\mu_0H_K$ with several different $\mu_0H_z/\mu_0H_C$, confirming that $J_S$ is inversely proportional to $\mu_0H_{DMI}/\mu_0H_K$. This result implies that a larger DMI reduces the switching current density by tilting the angle of chiral spin alignment at the pattern edges. By estimation of the temperature rise due to the current injection, our findings are basically free from artefacts caused by Joule heating (see Note 5 of the Supplemental Material [20]).

### C. Possible reason for tendency of $\mu_0H_K$ and $\mu_0H_{DMI}$ with $t_{Cu}$

Herein, we would like to clarify the possible reason for the tendency of $\mu_0H_K$ with $t_{Cu}$ and of $\mu_0H_{DMI}$ with $t_{Cu}$. First, the increase in $\mu_0H_K$ as $t_{Cu}$ rises originates from preventing intermixing between Co and Pt by inserting an ultrathin Cu layer. Despite strong PMA at Pt/Co interface, it can be weakened by a low quality of interface, caused by intermixing or interdiffusion [11]. The introduction of the Cu layer prevents intermixing due to its immiscibility with Co, resulting in high quality of interface [26], while preserving the spin information from Pt through Cu due to its long spin diffusion length [27,28], resulting in larger $\mu_0H_K$ [12]. Second, the emergence of enhanced $\mu_0H_{DMI}$ as $t_{Cu}$ increases is attributed to the spatial inversion symmetry breaking by inserting a Cu layer at the symmetric Pt/Co/Pt heterostructure. The subsequential increase of $\mu_0H_{DMI}$ arises from the contribution of the second nearest neighbor, in addition to the that of the nearest neighbor [29]. Therefore, by increasing the Cu layer, the simultaneous enhancement of $\mu_0H_K$ and $\mu_0H_{DMI}$ was achieved.

## IV. CONCLUSION

In summary, we propose here a solution to simultaneously achieve both the thermal stability enhancement and the switching current reduction in magnetic devices driven by spin torque. By employing a Cu insertion layer in Pt/Co/Cu/Pt layers, both the PMA and DMI are enhanced. A large PMA directly enhances the thermal stability; a large DMI generates noncollinear spin alignment at the pattern edges, and consequently reduces the switching current density. Our results show that effective DMI engineering provides both stable data retention and energy-efficient operation suitable for spintronic applications.

## ACKNOWLEDGMENTS

This work was supported by the KIST Institutional Program (Grants No. 2E31541, No. 2E32251, and No. 2E32951) and the National Research Foundation of Korea (NRF) program (NRF-2022M3I7A2079267) funded by Ministry of Science and ICT. Y.-K.P., J.-S.K., Y.-S.N., J.-S.Y., and S.-B.C. were supported by Samsung Electronics Co., Ltd., the Samsung Science & Technology Foundation (Grant No. SSTF-BA1802-07), and the NRF program (Grant No. 2020R1A5A1016518). D.H.K. and M.K. were supported by the NRF program (Grant No. NRF-2022R1A2C2004493).

[1] J. C. Slonczewski, J. Magn. Magn. Mater. **159**, L1 (1996).
[2] S. Fukami and H. Ohno, Jpn. J. Appl. Phys. **56**, 0802A1 (2017).
[3] J. Ryu, S.-B. Choe, and H.-W. Lee, Phys. Rev. B **84**, 075469 (2011).
[4] A. Thiaville, S. Rohart, É. Jué, V. Cros, and A. Fert, Europhys. Lett. **100**, 57002 (2012).
[5] A. Manchon, J. Železný, I. M. Miron, T. Jungwirth, J. Sinova, A. Thiaville, K. Garello, and P. Gambardella, Rev. Mod. Phys. **91**, 035004 (2019).
[6] J. Hayakawa, S. Ikeda, Y.-M. Lee, R. Sasaki, T. Meguro, F. Matsukura, H. Takahashi, and H. Ohno, Jpn. J. Appl. Phys. **45**, L1057 (2006).
[7] D.-S. Han, N.-H. Kim, J.-S. Kim, Y. Yin, J.-W. Koo, J. Cho, S. Lee, M. Kläui, H. J. M. Swagten, B. Koopmans, and C.-Y. You, Nano Lett. **16**, 4438 (2016).
[8] N. Mikuszeit, O. Boulle, I. M. Miron, K. Garello, P. Gambardella, G. Gaudin, and L. D. Buda-Prejbeanu, Phys. Rev. B **92**, 144424 (2015).
[9] S. Pizzini, J. Vogel, S. Rohart, L. D. Buda-Prejbeanu, E. Jué, O. Boulle, I. M. Miron, C. K. Safeer, S. Auffret, G. Gaudin, and A. Thiaville, Phys. Rev. Lett. **113**, 047203 (2014).
[10] P.-H. Jang, K. Song, S.-J. Lee, S.-W. Lee, and K.-J. Lee, Appl. Phys. Lett. **107**, 202401 (2015).

[11] S. Bandiera, R. C. Sousa, B. Rodmacq, and B. Dieny, IEEE Magn. Lett. **2**, 3000504 (2011).
[12] S. Bandiera, R. C. Sousa, B. Rodmacq, and B. Dieny, Appl. Phys. Lett. **100**, 142410 (2012).
[13] A. K. Chaurasiya, C. Banerjee, S. Pan, S. Sahoo, S. Choudhury, J. Sinha, and A. Barman, Sci. Rep. **6**, 32592 (2016).
[14] N.-H. Kim, J. Jung, J. Cho, D.-S. Han, Y. Yin, J.-S. Kim, H. J. M. Swagten, and C.-Y. You, Appl. Phys. Lett. **108**, 142406 (2016).
[15] E. C. Stoner and E. P. Wohlfarth, Philos. Trans. R. Soc. **240**, 599 (1948).
[16] H.-S. Whang, S.-J. Yun, J. Moon, and S.-B. Choe, J. Magn. **20**, 8 (2015).
[17] S. Okamoto, N. Kikuchi, O. Kitakami, T. Miyazaki, Y. Shimada, and K. Fukamichi, Phys. Rev. B **66**, 024413 (2002).
[18] S. Emori, U. Bauer, S.-M. Ahn, E. Martinez, and G. S. D. Beach, Nat. Mater. **12**, 611 (2013).
[19] Y.-K. Park, D.-Y. Kim, J.-S. Kim, Y.-S. Nam, M.-H. Park, H.-C. Choi, B.-C. Min, and S.-B. Choe, NPG Asia Mater. **10**, 995 (2018).
[20] See Supplemental Material at http://link.aps.org/supplemental/10.1103/PhysRevMaterials.8.044405 for the detailed measurement method and analysis used in Fig. 1; the validation of the presence of Néel-type DWs in all film series; the measurement of Λ via the change of coercivity μ0HC with respect to dμ0Hz/dt; the detailed description of the domain nucleation at the edge with various current and domain polarities; and the estimation of the temperature rise due to the current injection caused by the Joule heating. The Supplemental Material also contains Refs. [30–36].
[21] J. Moritz, B. Dieny, J. P. Nozières, Y. Pennec, J. Camarero, and S. Pizzini, Phys. Rev. B **71**, 100402(R) (2005).
[22] W. Wernsdorfer, B. Doudin, D. Mailly, K. Hasselbach, A. Benoit, J. Meier, J.-Ph. Ansermet, and B. Barbara, Phys. Rev. Lett. **77**, 1873 (1996).
[23] B. Barbara, J. Magn. Magn. Mater. **129**, 79 (1994).
[24] S.-G. Je, D.-H. Kim, S.-C. Yoo, B.-C. Min, K.-J. Lee, and S.-B. Choe, Phys. Rev. B **88**, 214401 (2013).
[25] F. Schumacher, J. Appl. Phys. **70**, 3184 (1991).
[26] T. Nishizawa and K. Ishida, Bull. Alloy Phase Diagrams **5**, 161 (1984).
[27] F. J. Jedema, A. T. Filip, and B. J. van Wees, Nature (London) **410**, 345 (2001).
[28] S. Mizukami, Y. Ando, and T. Miyazaki, Phys. Rev. B **66**, 104413 (2002).
[29] H. Yang, A. Thiaville, S. Rohart, A. Fert, and M. Chshiev, Phys. Rev. Lett. **115**, 267210 (2015).
[30] P. P. J. Haazen, E. Murè, J. H. Franken, R. Lavrijsen, H. J. M. Swagten, and B. Koopmans, Nat. Mater. **12**, 299 (2013).
[31] S. Emori, E. Martinez, K.-J. Lee, H.-W. Lee, U. Bauer, S.-M. Ahn, P. Agrawal, D. C. Bono, and G. S. D. Beach, Phys. Rev. B **90**, 184427 (2014).
[32] J. H. Franken, M. Herps, H. J. M. Swagten, and B. Koopmans, Sci. Rep. **4**, 4248 (2014).
[33] D.-Y. Kim, D.-H. Kim, and S.-B. Choe, Appl. Phys. Express **9**, 053001 (2016).
[34] D.-H. Kim, S.-C. Yoo, D.-Y. Kim, B.-C. Min, and S.-B. Choe, Sci. Rep. **7**, 45498 (2017).
[35] S.-G. Je, S.-C. Yoo, J.-S. Kim, Y.-K. Park, M.-H. Park, J. Moon, B.-C. Min, and S.-B. Choe, Phys. Rev. Lett. **118**, 167205 (2017).
[36] K.-J. Kim, J.-C. Lee, S.-B. Choe, and K.-H. Shin, Appl. Phys. Lett. **92**, 192509 (2008).